Dynamic Aperture and Frequency Map Analysis of the Synchrotron Radiation Source

Dean Markwick and Susheel Adusumilli
©2014

Abstract

An electron beam in the Synchrotron Light Source was tracked by analysing the beam dynamics through a Poincaré section of the accelerator. The inherent non-linearities of such a system are discussed and the properties of the beam are computed using an iterative method. The β function was computed and agreed with the known function shape. The dynamic aperture was calculated to be $|x| = 2 \pm 0.5$cm and $|y| = 4 \pm 0.5$cm. The working point of the system was shown to be isolated from low order resonances. The Figenbaum constant was also calculated as 4.3 ± 0.2. The errors in the calculations mainly arise from the iterative step size used.

1   Introduction

In non-linear dynamical systems, there is usually a transition from periodic behaviour to chaos, where small changes in initial conditions can lead to very different final values. Such effects exist in particle accelerators, and techniques are needed to quantify and restrict these effects, because particles in the beam can acquire transverse amplitudes so large that they hit the vacuum chamber surrounding the beam and are lost. Such non-linear effects introduce an upper bound on the initial amplitudes of the particles in the system. This upper bound is called the dynamic aperture. This must be maximised in order to contain as many particles as possible within the beam.

Here, we start by exploring a very simple accelerator system, where a particle experiences a small kick each time it passes through a RF cavity. This system is dynamically similar to a mathematical system called the Standard Map [1], and a study of this system can provide a basic understanding about the concepts of phase space, and different ways of exploring the non-linear dynamics of the system.

The accelerator system explored here is the now-closed Synchrotron Radiation Source in Daresbury, which has a circumference of 96m and operates at an energy of 2GeV. The non-linear effects here are mainly due to sextupole magnets, which are used to focus the beam. Electrons with different starting amplitudes are tracked over a large number of turns and the amplitudes of the particles are tracked to measure the dynamic aperture. The main use of a synchrotron source is to provide radiation emitted from the electrons. This reduces the amplitudes of the electrons, but this effect is much less in proton accelerators, and analysis of the system over a large number of turns becomes more important. However, it is shown in [4] by the introduction of a method called Frequency Map Analysis that the Australian Light Source would benefit from such tracking, which resulted in an increase of the dynamic aperture, and similar methods are applied for the SRS here. Frequency map analysis mostly utilises the tracking code developed for calculating the dynamic aperture, and incorporates refined Fourier techniques, and hence is an easy and effective way of maximising the dynamic aperture.

2   The Standard Map and Chaos

Phase space is a co-ordinate system in which a dynamical system can be represented. The usual Cartesian co-ordinates (x, y), are replaced with (x, x'), where x' is the velocity of the particle. This allows us to explore different properties of motion. For example, in simple harmonic motion, the phase space diagram corresponds to an ellipse. The semi-major axis signifies the amplitude of the motion, therefore the area of the ellipse is proportional to the energy of the system. For simple harmonic motion, the energy of the system is defined as

$$E = \frac{1}{2}kA^2, \tag{1}$$

where A is the amplitude of the system and k is a constant. This means that each ellipse of distinct area in phase space represents a unique system with a certain amount of energy. For energy to be conserved, phase space trajectories are incompressible. This mathematically is Liouvelle's theorem, the volume of space that the particles occupy in the phase space is constant.

We extend the analysis of phase space dynamics and now consider the standard map, whose equations are given by:

$$
\begin{aligned}
x_{n+1} &= x_n + x'_{n+1}, && (2) \\
x'_{n+1} &= x'_n + K\sin(x_n). && (3)
\end{aligned}
$$

This, physically, is the integrated equations of motion for a kicked pendulum, or the motion of particles in an accelerator with a small RF cavity kick. The pendulum is constrained to move in one dimension (x) and receives a kick of magnitude K, periodically.

The resulting phase space diagram produces the standard map (Chirikov-Taylor map).

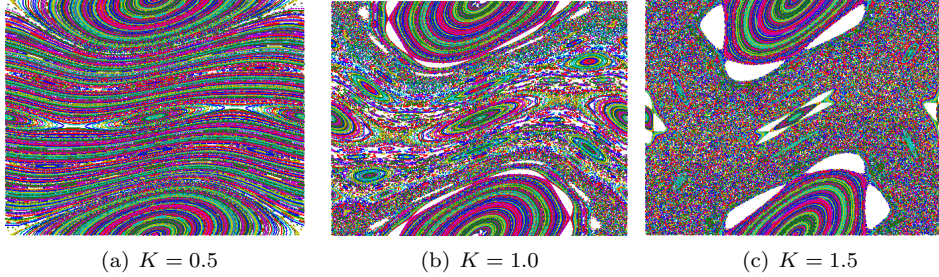(a) $K = 0.5$ (b) $K = 1.0$ (c) $K = 1.5$

Figure 1: Increasing the strength of the driving force K increases the disorder of the system. These diagrams have been computed in MATLAB.

For small enough starting x' values (at the centre of the map), the resulting trajectories are ellipses, indicating that the motion is bound. Once the starting velocity is larger than a critical value, unique for each K value, the paths become curves. This indicates that the motion is no longer bound. For large enough K values, as demonstrated in figure 1(c), clear curves are no longer visible, and the pattern resembles noise. This indicates chaotic motion.

Within an accelerator, bound motion is essential. It allows the particles that are being accelerated to be monitored and controlled accordingly. Chaotic and unbounded motion would lead to total decay of the beam with which it is impossible to perform experiments with. Here, the effects accelerator components have on the phase space diagrams were investigated with the overall aim to maximise the dynamic aperture.

2.1 Quantifying Chaos

There is no general method of quantifying chaos, but there is commonly a region in phase space where long term periodic motion changes to a system with high sensitivity on initial conditions. In the region of chaos, we can see that a small change in initial conditions can give a different final values after tracking the system for some time. We observe and quantify this transition from periodic to chaotic motion using two methods.

Firstly, by calculating the frequency of the particles with a given starting point in phase space using a Fourier transform algorithm. All stable orbits have the same frequencies as is expected in simple harmonic oscillation. However, in a region of chaos, there is no discernible relationships between frequencies measured as K is increased.
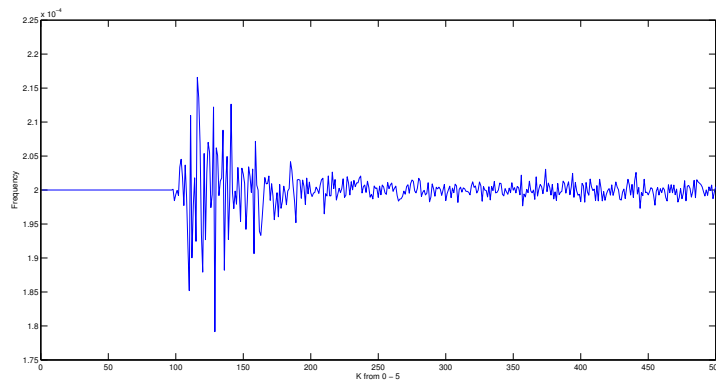

Figure 2: Frequencies vs. K plot for the standard map. The chaotic region starts when the frequency is no longer constant.

Another method of quantifying chaos directly exploits one of the definitions of chaos; that small perturbations on initial conditions can lead to significantly different results. Here, we track two paths with close initial starting conditions. The limit on difference in paths in 'double' variables in MATLAB is $2^{-52} \equiv 10^{-16}$

In this instance, we separate the two starting values by a distance of 10^{-6}. By approximating a relation $|D(t)| \equiv e^{\lambda t}|D(0)|$ and by measuring λ, the Lyapunov exponent, we have a way of measuring the separation of the two paths after a sufficiently long time [10]. However, there is a potential danger of the two paths moving too close or too far from each other that it is beyond the precision used in the software package. This can be fixed using the ergodic hypothesis, which states that "a time average along a single representative trajectory is equivalent to a spatial average over the attractor, weighted by the density of points on the attractor" [9] (Sprott, 2006). Hence by, adjusting the distance between two paths after each iteration, so that the paths don't stray by a large amount, and averaging this over time (number of iterations), we essentially measure a spatial average over the attractor. Implementing the two techniques above for the standard map, figure 3 was obtained.
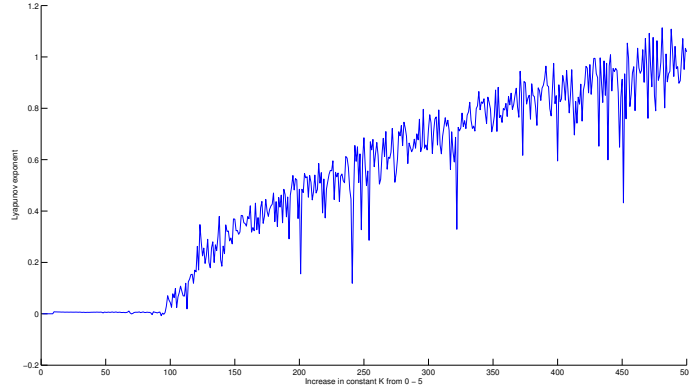

Figure 3: Lyapunov exponent plot for different K values in the standard map. We can see that both methods give the same starting points for the chaotic regions. The dips in the Lyapunov exponents are due to the formation of islands in phase space in figure 1

3 Synchrotron Light Sources

Synchrotron Light sources use a bending magnet (the wedge bend) to guide the particle on a circular trajectory, in the SRS, the radius is 96m. There are 16 sections consisting of a combination of magnets in the SRS. Each section is called a lattice. As the particle beam is guided along the trajectory, it tends to disperse, i.e. they stray away from the desired orbit. In order to control the dispersion, it becomes necessary to focus the beam using quadrupole magnets [11].

A quadrupole can be de-constructed into two fields, see figure 4(a). It focuses in one direction and defocuses in the other because it can provide a field linearly proportional to the offset of the particle at the centre of the magnet.

$$B_x \quad \propto \quad -x, \tag{4}$$
$$B_y \quad \propto \quad y. \tag{5}$$

Each quadrupole has a characteristic focal length f. By using two quadrupoles with focal lengths f_1 and f_2, and by specifying distance d between the two quadrupoles, we can provide an overall focusing effect though the equation $1/f_{total} = 1/f_1 + 1/f_2 - d/f_1 f_2$, even when f_1 and f_2 have different signs [11]. The solutions of the equations of motion (similar to simple harmonic motion, since the there is a linear restoring force) of the beam as it goes through the quadrupole can be represented as a 4x4 matrix.

However, the deflection of the beam by quadrupole magnets is linear only in the first approximation, but in reality the deflection of the beam is dependent on particle energy, resulting in chromaticity. In order to focus all particles to the same point, we need magnets providing higher-order focusing terms, provided by sextupole magnets, which have provide a field of 2nd order (x^2). But, this field is non-linear and the inherent chaos in non-linear beam dynamics compromise the stability of the beam, especially at high amplitudes. The particle positions and velocities can be determined using non-linear transformations governed by the equations (6) – (9).

The quadrupoles and sextupoles are placed between the bending magnets on the straight sections. The order of the magnets placed on the straight sections in the SRS is called a FODO (Focusing Defocusing) lattice. The empty spaces between the magnets are called drift spaces, and the equations of motion can be represented as a 4x4 matrix.

The beam is bent by a dipole magnet, called the wedge bend, which gives raise to dispersion only in the x direction in which the beam is bent. In the other direction y, it is a drift space.

3

$$
\begin{align}
x_{n+1} &= x_n, \tag{6}\\
x'_{n+1} &= x'_n - \frac{kL}{2}(x_n^2 - y_n^2), \tag{7}\\
y_{n+1} &= y_n, \tag{8}\\
y'_{n+1} &= kLx_ny_n. \tag{9}
\end{align}
$$

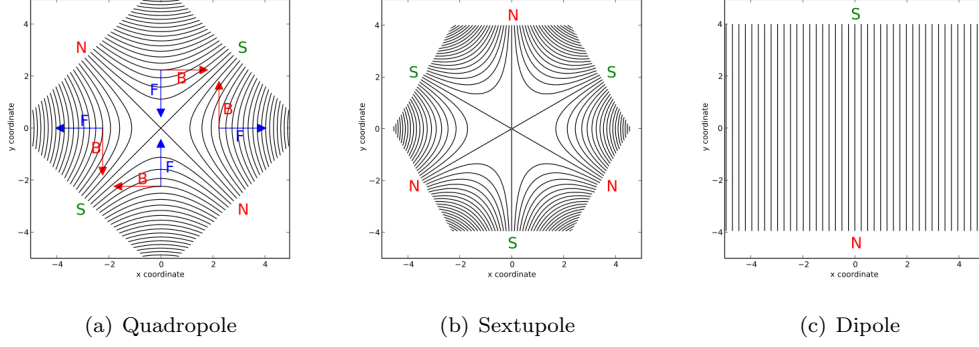(a) Quadropole   (b) Sextupole   (c) Dipole

Figure 4: The field lines for the magents used in the Daresbury light source. The normalised magnetic field gradient is denoted as k, it has unique values for each of the magnets.

The matrices in which transforms the particle velocities and positions as they pass though all the magnets used:

Focussing quadrupole, QF

$$
\begin{pmatrix} x_{n+1} \\ x'_{n+1} \\ y_{n+1} \\ y'_{n+1} \end{pmatrix} = \begin{pmatrix} x_n \\ x'_n \\ y_n \\ y_n \end{pmatrix} \begin{pmatrix} \cos(kL) & -k\sin(kL) & 0 & 0 \\ \frac{1}{k}\sin(kL) & \cos(kL) & 0 & 0 \\ 0 & 0 & \cosh(kL) & k\sinh(kL) \\ 0 & 0 & \frac{1}{L}\sinh(kL) & \cosh(kL) \end{pmatrix}
$$

Defocussing quadrupole, QD

$$
\begin{pmatrix} x_{n+1} \\ x'_{n+1} \\ y_{n+1} \\ y'_{n+1} \end{pmatrix} = \begin{pmatrix} x_n \\ x'_n \\ y_n \\ y_n \end{pmatrix} \begin{pmatrix} \cosh(kL) & k\sinh(kL) & 0 & 0 \\ \frac{1}{L}\sinh(kL) & \cosh(kL) & 0 & 0 \\ 0 & 0 & \cos(kL) & -k\sin(kL) \\ 0 & 0 & \frac{1}{k}\sin(kL) & \cos(kL) \end{pmatrix}
$$

Dipole, BD

$$
\begin{pmatrix} x_{n+1} \\ x'_{n+1} \\ y_{n+1} \\ y'_{n+1} \end{pmatrix} = \begin{pmatrix} x_n \\ x'_n \\ y_n \\ y'_n \end{pmatrix} \begin{pmatrix} \cos(\theta) & -\frac{\theta}{L}\sin(\theta) & 0 & 0 \\ \frac{L}{\theta}\sin(\theta) & \cos(\theta) & 0 & 0 \\ 0 & 0 & 1 & 0 \\ 0 & 0 & L & 1 \end{pmatrix}
$$

Free Space, D_i

$$
\begin{pmatrix} x_{n+1} \\ x'_{n+1} \\ y_{n+1} \\ y'_{n+1} \end{pmatrix} = \begin{pmatrix} x_n \\ x'_n \\ y_n \\ y'_n \end{pmatrix} \begin{pmatrix} 1 & 0 & 0 & 0 \\ L & 1 & 0 & 0 \\ 0 & 0 & 1 & 0 \\ 0 & 0 & L & 1 \end{pmatrix}
$$

Where k is the normalised field gradient, L is the length of the element. θ is the bending angle of the dipole.

4 The Simulation

The linear magnets, when represented by matrices, act as mapping functions of a particles position and velocity. Therefore progression through the accelerator system is achieved through successive multiplication of the matrices.

Initially, the sextupoles and dipole were treated as free space, this allowed for one matrix to be computed that represented one iteration through the accelerator. The components were also split up into the x direction and y direction:

$$
R_{Tx} = D_1 * QF * D_2 * QD * D_3 * D_4. \tag{10}
$$

$$
R_{Ty} = D_1 * QD * D_2 * QF * D_3 * D_4. \tag{11}
$$

Using the numerical values from the data book [6] and computing the resulting 1-turn matrix, a number of properties of the system can be calculated.

These matrices are periodic and can represented as a series of sines and cosines [7],

$$R_T \equiv M = \begin{pmatrix} \cos \mu + \alpha(s) \sin \mu & \beta(s) \sin \mu \\ -\gamma(s) \sin \mu & \cos \mu - \alpha(s) \sin \mu \end{pmatrix}, \tag{12}$$

from which it can be seen that the trace of M must be less than 2 for stable motion to exist [3]. This property allows construction of the formulae for $\beta(s)$.

$$\mu = \arccos \left(\frac{R_T(1,1) + R_T(2,2)}{2} \right), \tag{13}$$

$$\beta_0 = \frac{R_T(1,2)}{\sin \mu}. \tag{14}$$

Where $R(i,j)$ is the value of the (i,j)th element in the matrix R. The β_0 value must now be propagated through the accelerator to produce $\beta(s)$.

The $\beta(s)$ function is a property of the magnets and their focussing ability. It is related to the physical size of the beam σ through

$$\sigma(s) = \sqrt{\epsilon \beta(s)}. \tag{15}$$

The width of the beam, $\sigma(s)$, is assumed to be Gaussian and proportional to the emittance [11] ϵ and $\beta(s)$ functions. It is an important parameter for accelerator systems as the beam dimensions can be defined at any point on orbit of the particle.

The initial value of $\beta(s)$ was calculated (β_0) to compare to the known value from the Light Source Data book and confirm that the methods being used are correct. The full function, $\beta(s)$ is calculated later.

Through the computation, the values of β_0 in the two transverse directions were:

$$\beta_{0x} = 9.5,$$
$$\beta_{0y} = 1.1.$$

When compared to the known values from the Light Source Data book [6], these values are sufficiently similar and sufficiently accurate for a preliminary analysis of the system.

Due to the non-linear force that the sextupole provides, a matrix cannot be used to propagate a particle through a sextupole. Instead, a function was created (S, S') and used when a sextupole 'kick' was needed. Both x and y directions were combined in a single matrix for this computation. This reduced the number of calculations needed.

$$R_T = D_1 * QD * D_2 * D_{3A} * S * D_{3B} * D_4 * D_{5A} * S' * D_{5B} * QF * D_6 * BD. \tag{16}$$

This is a more accurate representation of the Daresbury Light Source and is the foundation for the further calculations. This lattice is repeated 16 times to complete one pass through the system.
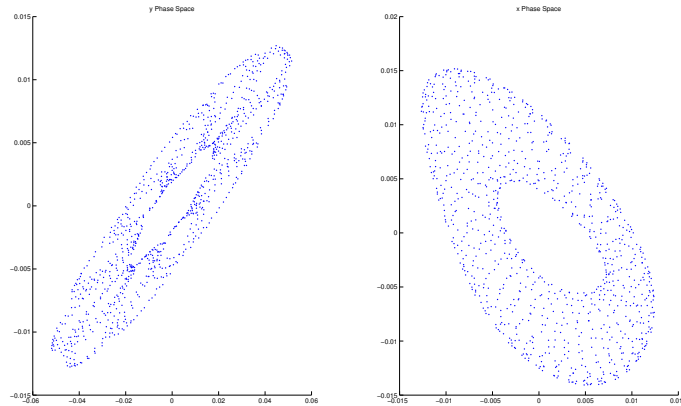

Figure 5: The phase diagram of both axis. In both the x and y direction the starting amplitude was 1cm. The sextupoles have induced a spread in the energy of the particle

The phase space diagrams computed, figure 5, are elliptical shape, which shows that the particles undergo simple harmonic motion within the accelerator. The width of the ellipses also shows how the spread of the energy of the particle varies within the accelerator.

The complete $\beta(s)$ function was calculated across the entire accelerator, thus, measuring the beam envelope as it passed through each component. The one turn matrix including the sextupoles, equation (16), could not be used to calculate the β value, as the calculation is dependent on linear dynamics. Therefore, the sextupoles were removed and a new one-turn matrix was calculated;

$$R_T = D1 * FQA * FQB * D2 * DFQA * DFQB * D3 * BD. \tag{17}$$

The quadrupoles, both focussing and defocussing, were split into two. This allowed for a value of β to be calculated within the middle of the magnet and a more accurate picture to be composed using equation (14). However, this equation only generates the final value of β. The matrix must be permuted cyclically, with each new combination featuring a new component at the start of the matrix. The ordering of the matrix was preserved.
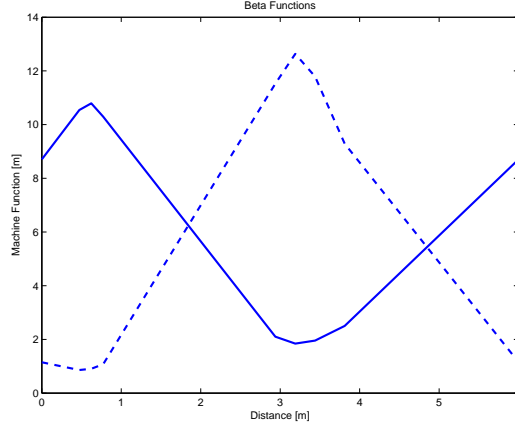

Figure 6: The value of β as the particle moves through the accelerator. It matches the known diagram [6], confirming further that the methods used are correct.

As expected, the value of β_x is a maximum at the x-focusing quadropole and minimum at the x-defocusing and vice versa. The β functions acts as a guide for the beam.

5 Dynamic Aperture and Frequency Map Analysis

Due to the resonance effects, certain particles would experience ever increasing amplitudes which would eventually lead to collisions with the walls of the accelerator. Their motion is no longer bound within the constraints of the accelerator.

There is now an optimisation to maximise the amplitude that can be found within the accelerator and still remain bound. This is commonly described as the dynamic aperture of the system.

To check whether that the particles motion was still bound, the particles x and y coordinate was analysed and confirmed to still exist. The matrices would produce a 'not a number' value if the particle escaped the constraining forces and was no longer bound. The particle would not orbit with a distinct frequency as it is in chaotic motion. This is an application of the methods seen in figure 2.

The distinction between bound and unbound motion can be related to the Standard Map, as seen in figure 1. Bound motion can be mapped as closed ellipses, figure 1(a). Unbound motion can be represented through open curves and disjointed points, mainly seen in figure 1(c). In the accelerator, K (equation (2)) is related to the magnitude of the sextupole strength. The sextupole provides the non-linear force and thus the entry to chaotic motion.

5.1 Dynamic Aperture

The starting amplitudes of the particles, i.e. x_0 and y_0 values, are a controlling parameter as to whether the particle remains bound through its iteration in the accelerator. The range of starting x and y values for which the motion remains stable (bound) within phase space is the dynamic aperture. It is key that the particle remains bound throughout the iterations through the accelerator.

For the given quadrupole and sextupole strengths [6], the starting amplitudes were varied as $x, y \leq |0.04|$m. All combinations of starting amplitudes in 0.001m steps were iterated through and tested to see if after passing through the accelerator 16000 times the motion remained bound. If it was still bound, the values of x_0 and y_0 were plotted onto their respective axis. If the motion was unstable, the starting values were discarded. This produced a 'swamp plot' and illustrates the range of values of which the particle can start with and still transverse through the accelerator.

Figure 7 is asymmetric, with a higher number of stable points for negative x. This is due to the direction in which the wedge bend matrix acts on the particle beam. It bends in the positive x direction, therefore,
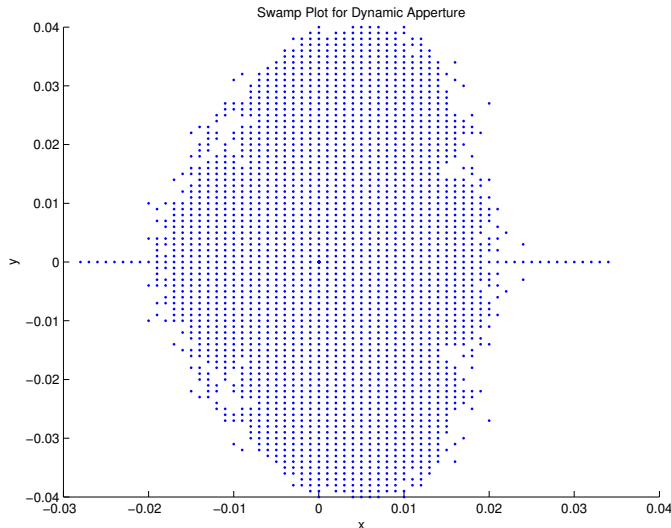
Figure 7: The stability region as expected there are higher regions of stability around the origin. As the starting values increase, the likelihood that it remains stable decreases. The maximum starting value of $|x|$ is 2cm and for $|y|$ it is 4cm. The straight line at $y = 0$ represents a perfect initial starting value, which is a physical impossibility, the particle will always have a slight offset.

particles with larger negative x_0 values will be moved closer towards the ideal path, the centre of the magnet. As the swamp plot shows, the paths closer to the ideal trajectory $x = 0, y = 0$, the more likely the particle will remain stable.

Again, the exploration of starting values can be seen as iterating through the standard map, figure 1, locating the regions where the motion is stable and thus a closed ellipse is located on the standard maps.

5.2   Frequency Map Analysis

The tune of an electron in a synchrotron is defined as the number of oscillations of the particle per turn and can be generated by integrating the inverse of the β function over the circumference

$$\nu = \frac{1}{2\pi} \oint \frac{ds}{\beta}, \tag{18}$$

where s is the distance measured from an arbitrary starting point. If there were no non-linearities, there would only be one set of tunes (horizontal and vertical), at the 'working point. However, due to the non-linearities arising from the second order sextupole fields, there are a range of possible tunes. It is known from Kolmogorov-Arnold-Moser theory that in the phase space we obtain for the accelerator, there exist many invariant tori which determine the motion of a particle, which shows quasi-periodic behaviour [4]. Each tori can be represented by a point in frequency space, and the regions between the tori are chaotic but the tori themselves act as a boundary to the chaotic regions, which move through the frequency map through fractal connections (Arnold diffusion). But, the diffusion falls off exponentially as particles approach the tori [5].

Due to the irregular periodic behaviour in the tori, refined Fourier methods need to be implemented to measure the tune. Here, we use an Interpolated Fourier-Hanning algorithm whose accuracy with number of iterations scales as $\frac{1}{N^4}$ rather than the $\frac{1}{N}$ accuracy obtained from the Fourier transform function in MATLAB [8].

Starting with x and y amplitudes from 0 - 2cm, we tracked the beam for a large number of turns, and measured the x and y tunes for the first half (ν_{x1} and ν_{y1}) the second half (ν_{x2} and ν_{y2}). The diffusion in tune $\sqrt{(\nu_{x1}^2 - \nu_{x2}^2) + (\nu_{y2}^2 - \nu_{y2}^2)}$ is transferred logarithmically onto a colour map. This is overlaid on to the ν_{x1} vs. ν_{y1} plot to obtain the frequency map, figure 8. We can see that although the tori exhibit low diffusion, the resonance frequencies on the tori are destroyed, which is why it is essential to move the working point of the synchrotron away from such resonances.
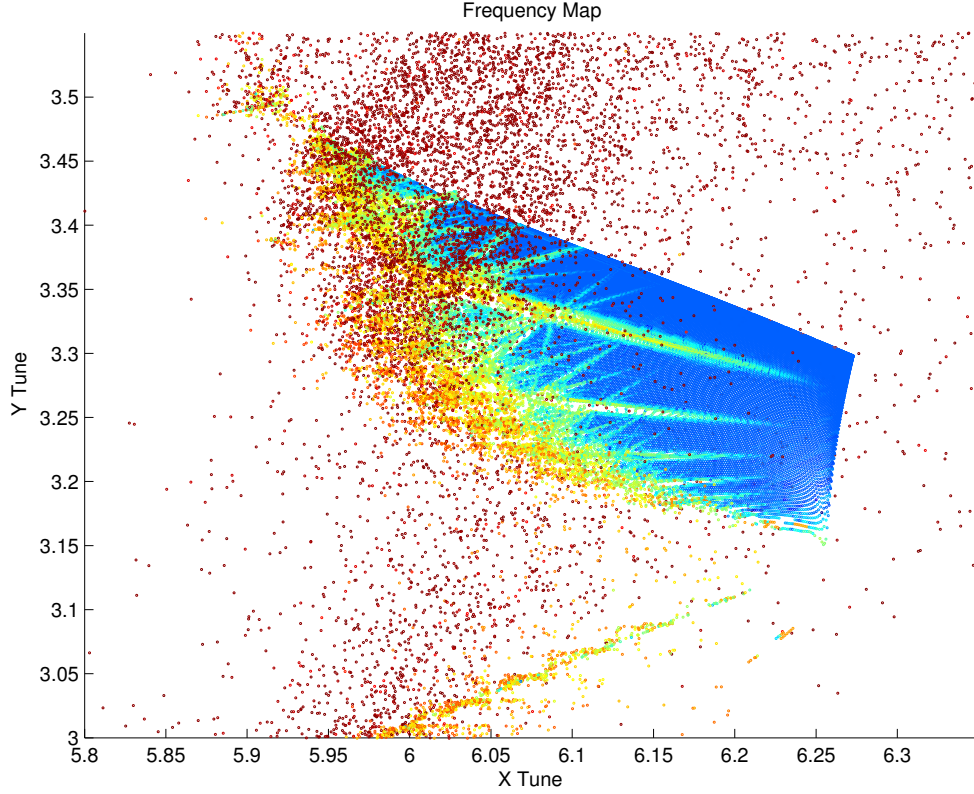
Figure 8: Frequency Map Analysis (FMA) for the SRS synchrotron. The tune diffusion is transferred onto a colour map - red if the tune diffusion is large and blue if the particles show long term stability

5.3 Resonances

The frequency map and dynamic aperture shows a number of lines cutting in and disrupting the overall structure of the plots. This is due to resonance effects that the magnets can have on the particles as they pass through the accelerator.

$$n\nu_x - m\nu_y = I \tag{19}$$

$$n\nu_x + m\nu_y = I \tag{20}$$

$$I, n, m \in \mathbb{N}$$

A difference resonance is one in which the motion remains bounded, equation (19). This is because the'kicking' effect that the resonance evokes is not large enough to move it to a new tori. Therefore, difference have no effects on the dynamic aperture of the particle. A sum resonance, equation (20), allows for the amplitude of the motion to continually grow and thus the energy of the particle increases. This allows it to jump into a new tori until it collides with the physically constraining wall and the particle is lost. Therefore, the working point must be located away from any sum resonances, so that particles do experience uncontrollable amplitude growth.

It is possible to draw the low order resonance lines for both the sum and difference. This was then traced over the frequency map and illustrates how the closest resonance lines are sufficiently distant from the working point and thus won't have a effect on the dynamic aperture.
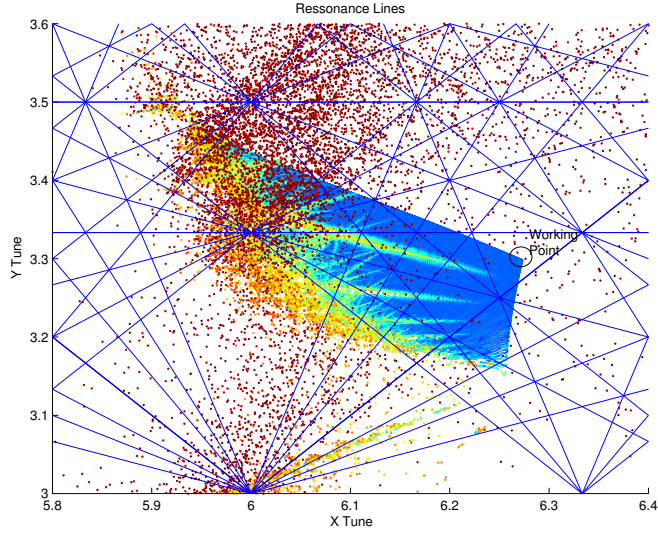
Figure 9: Sum and difference resonance lines up to orders $I \leq 9$. As expected, large amounts of disruption can be seen at $\nu_x = 6$ for all ν_y values, this is due to multiple resonance lines crossing. The labelled working point is isolated from any resonance lines.

5.4 Figenbaum Constant

It is known that the transition from periodicity to chaos occurs through a series of period-doubling bifurcations, where a simple sine wave oscillating between two values starts oscillating between four values, then eight and so on until the frequency has no general pattern. With a given starting amplitude, by increasing the sextupole strength, which governs the non-linearity of the system, we find such a boundary between periodicity and chaos and we assume that such behaviour is consistent with period doubling bifurcations. A general property governing the period doubling bifurcations is that by measuring the bifurcation parameter α (which relates to the sextupole strengths), we arrive at the Figenbaum constant F determined by the expression

$$F = \lim_{n \to \infty} \frac{\alpha_{n-1} - \alpha_{n-2}}{\alpha_n - \alpha_{n-1}}. \tag{21}$$

We measured only the first two terms in the converging sequence and arrived at a value of 4.3 ± 0.2 . The true value at the limit as $n \to \infty$ is 4.669 [2].
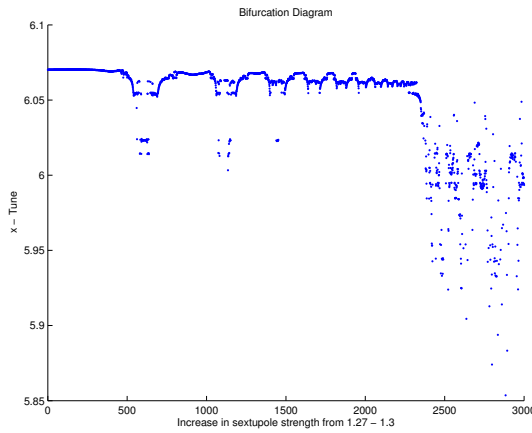

Figure 10: Plot of the x-tune vs.sextupole strength for the accelerator system. There is a chaotic region at high sextupole strengths and a stable tune for low strengths.

9

6 Conclusion

The dynamic aperture has been successfully demonstrated as $|x| = 2$cm and $|y| = 4$cm. Using frequency map analysis, the working point of the accelerator has been shown in isolation away from low order resonance lines. Frequency map analysis, a tool initially developed to understand the chaotic dynamics of the solar system, is an invaluable resource providing a 'finger print' which is unique to each accelerator. The accuracy of all values can be refined through increasing the iterative step size.

References

[1] Alexander Wu Chao and Maury Tigner. *Handbook of Accelerator Physics and Engineering.* World Scientific, 3 edition, 2006.

[2] P. Smith D.W. Jordan. *Non-Linear Ordinary Differential Equations: Introduction for Scientists and Engineers.* Oxford University Press, 2007.

[3] Bernhard Holzer. Introduction to transverse beam optics: Twiss parameters & lattice design. Technical report, CERN, 2009.

[4] J Laskar and D Robin. Application of frequency map analysis of the als. Technical report, Lawrence Berkeley Lab., CA (United States), 1996.

[5] Alessandro Morbidelli and Antonio Giorgilli. Superexponential stability of kam tori. *J. Statist. Phys*, 78:1607–1617, 1995.

[6] James B. Murphy. *Synchrotron Light Source Data Book.* BNL/NSLS, 1989.

[7] Hywel Owen. Lattice design codes. Technical report.

[8] Hywel Owen. Tune evaluation using hanning filters. Technical Report DPG-XX-rpt-009, CLRC Daresbury Laboratory, U.K, 2001.

[9] Julien C. Sprott. *Elegant Chaos.* World Scientific, 2006.

[10] Julien Clinton Sprott and Julien C Sprott. *Chaos and time-series analysis*, volume 69. Oxford University Press Oxford, 2003.

[11] H. Weidemann. *Particle Accelerator Physics I.* Springer, 2001.

A Appendix